Mechanistic Studies of Ubiquitin C-Terminal Hydrolase L1

April Case and Ross L. Stein*

Laboratory for Drug Discovery in Neurodegeneration, Harvard Center for Neurodegeneration and Repair, 65 Landsdowne Street, Fourth Floor, Cambridge, Massachusetts 02139

Received October 19, 2005; Revised Manuscript Received January 4, 2006

ABSTRACT: Ubiquitin C-terminal hydrolases (UCHs) cleave Ub−X bonds (Ub is ubiquitin and X an alcohol, an amine, or a protein) through a thioester intermediate that is produced by nucleophilic attack of the Cys residue of a Cys-SH/His-Im catalytic diad. We are studying the mechanism of UCH-L1, a UCH that is implicated in Parkinson's disease, and now wish to report our initial findings. (i) Pre-steady-state kinetic studies for UCH-L1-catalyzed hydrolysis of Ub-AMC (AMC, 7-amido-4-methylcoumarin) indicate that k_{cat} is rate-limited by acyl-enzyme formation. Thus, $K_m = K_s$, the dissociation constant for the Michaelis complex, and $k_{cat} = k_2$, the rate constant for acyl-enzyme formation. (ii) For K_{assoc} ($=K_s^{-1}$), $\Delta C_p = -0.8$ kcal mol^{-1} deg^{-1} and is consistent with coupling between substrate association and a conformational change of the enzyme. For k_2, $\Delta S^{\ddagger} = 0$ and suggests that in the E−S, substrate and active site residues are precisely aligned for reaction. (iii) Solvent isotope effects are $^{D}K_{assoc} = 0.5$ and $^{D}k_2 = 0.9$, suggesting that the substrate binds to a form of free enzyme in which the active site Cys exists as the thiol. In the resultant Michaelis complex, the diad has tautomerized to ion pair Cys-S$^-$/His-ImH$^+$. Subsequent attack of thiolate produces the acyl-enzyme species. In contrast, isotope effects for association of UCH-L1 with transition-state analogue ubiquitin aldehyde suggest that an alternative mechanistic pathway can sometimes be available to UCH-L1 involving general base-catalyzed attack of Cys-SH by His-Im.

Deubiquitinating enzymes comprise a large family of enzymes that specifically cleave ubiquitin-derived substrates of the general structure Ub$^{1-72}$-Leu^{73}-Arg^{74}-Gly^{75}-Gly^{76}-X, where X can be any number of leaving groups ranging from small thiols and amines to Ub and other proteins (*1*−*4*). While at least five families of DUBs[1] have been identified (*4*), the two largest and best characterized are the UCHs and the UBPs. UBPs are generally high-molecular mass enzymes (∼100 kDa) and cleave substrates where X is a protein or another molecule of Ub. These enzymes are thought to have domains adjacent to the primary Ub substrate binding site that can recognize and bind these proteinacious leaving groups. Perhaps the most thoroughly studied UBP is isopeptidase T (*5*−*7*) which cleaves substrates where X is Ub. In contrast, UCHs are low-molecular mass enzymes (∼30 kDa) and hydrolyze Ub derivatives where X is a thiol or an amine and are thought not to have a binding domain for protein leaving groups.

Both UBPs and UCHs are cysteine hydrolases and catalyze the hydrolysis of amide bonds of their substrates according to the three-step mechanism of Scheme 1. In the first step, substrate and enzyme combine to form the Michaelis complex. From within this complex, the sulfhydryl of the active site cysteine attacks the carbonyl carbon of the amide bond of the substrate to generate an acyl-enzyme intermediate and liberate the first product. Finally, hydrolysis of the acyl-enzyme intermediate produces the reaction's second product Ub and regenerates free enzyme. For this mechanism, the steady-state rate parameters k_c/K_m, k_c, and K_m are related to the mechanistic rate parameters K_s, k_2, and k_3 as shown in eqs 1−3.

Scheme 1: Minimal Kinetic Mechanism for Ubiquitin C-Terminal Hydrolases

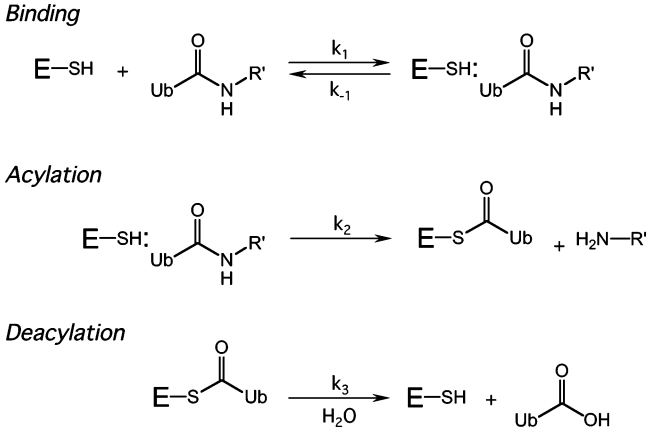

$$\frac{k_c}{K_m} = \frac{k_2}{K_s} \quad (1)$$

$$k_c = \frac{k_2 k_3}{k_2 + k_3} \quad (2)$$

$$K_m = K_s\left(\frac{k_3}{k_2 + k_3}\right) \quad (3)$$

* To whom correspondence should be addressed: Laboratory for Drug Discovery in Neurodegeneration, Harvard Center for Neurodegeneration and Repair, 65 Landsdowne St., Fourth Floor, Cambridge, MA 02139. Phone: (617) 768-8651. Fax: (617) 768-8606. E-mail: rstein@rics.bwh.harvard.edu.

[1] Abbreviations: AMC, 7-amido-4-methylcoumarin; Ub, ubiquitin; Ub-H, C-terminal aldehyde of Ub; DUB, deubiquitinating enzyme; UCH, ubiquitin C-terminal hydrolase; UBP, ubiquitin-specific processing enzyme; DTT, dithiothreitol; FI, fluorescence intensity.

10.1021/bi052135t CCC: $33.50
Published on Web 01/31/2006

In these expressions, $K_s = (k_{-1} + k_2)/k_1$, which for hydrolyses of most amides can be simplified to $K_s = k_{-1}/k_1$.

Our interest in these enzymes originates in the potential involvement of a particular one, UCH-L1, in Parkinson's disease (*8*−*10*) and cancer (*11*−*13*). As part of an ongoing program of drug discovery research to identify modulators of the enzymatic activity of UCH-L1 (*13*), we have initiated studies to characterize critical features of this enzyme's mechanism.

MATERIALS AND METHODS

General. Buffer salts and deuterium oxide were from Sigma Chemical Co. Ub-AMC (Boston Biochem, Inc., Cambridge, MA) was received as a 450 μM stock solution in DMSO. It was diluted to 45 μM in DMSO and stored as aliquots at −80 °C. UCH-L1 (Boston Biochem) was received as a 100 μM stock, diluted to 10 and 1 μM in a pH 7.6 buffer of 50 mM HEPES, 100 mM NaCl, 0.5 mM EDTA, 0.5 mg/mL ovalbumin, and 5 mM DTT, and stored at −80 °C as aliquots. Ub-H (Boston Biochem) was received as 50 μg of a lyophilized powder which was stored at −20 °C until it was used. The powder was reconstituted in 59 μL of the buffer described above to yield a 100 μM solution. Dilutions of this to 10 and 1 μM were made, and all these solutions were stored at −80 °C until they were used.

Buffer Salts for pH Dependencies. In all of these kinetic studies, reaction solutions contained 50 mM buffer salt, 500 mM NaCl, 0.5 mM EDTA, 0.1 mg/mL ovalbumin, 1 mM DTT, and 1% DMSO. The following buffer salts were used: MES ($pK_a = 6.2$) at pH 5.5−6.5, PIPES ($pK_a = 6.8$) at pH 6.5−7.0, HEPES ($pK_a = 7.5$) at pH 7.0−8.0, HEPBS ($pK_a = 8.3$) at pH 8.5−9.0, and CHES ($pK_a = 9.3$) at pH 9.5−10.0.

General Kinetic Methods. In a typical kinetic run, 390 μL of assay buffer was added to a 1 mL fluorescence cuvette and the cuvette placed in the jacketed cell holder of a Hitachi 4500 fluorescence spectrophotometer. The reaction temperature was maintained at 25.0 ± 0.02 °C by a circulating water bath. After the reaction solution had reached thermal equilibrium (~5 min), 1−10 μL of the stock enzyme solution was added to the cuvette. The reaction solution was incubated for an additional 30 min to allow DTT-mediated activation of UCH-L1 before the addition of 10 μL of a substrate solution in DMSO. Reaction progress was monitored by the increase in fluorescence emission at 460 nm ($\lambda_{ex} = 380$ nm) that accompanies cleavage of AMC from Ub-AMC. For each kinetic run, 200−1000 data points, corresponding to [time, FI] pairs, were collected by a computer interfaced with the fluorescence spectrophotometer.

These reactions are also studied using a Molecular Devices Gemini XS microplate spectrofluorometer. This allowed multiple reactions to be followed simultaneously with little decrease in the quality of data relative to the Hitachi F4500 fluorometer.

Titration of UCH-L1 with Ubiquitin Aldehyde. To determine the steady-state dissociation constant for the inhibition of UCH-L1 by Ub-H, we conducted enzyme titration experiments in which residual activity was measured for enzyme reaction solutions in which $[I]_o \sim [E]_o > K_i$. Specifically, 2.0 mL reaction solutions containing 10 nM UCH-L1 and various concentrations of Ub-H were allowed to incubate at 25.0 ± 0.02 °C for 2 h. At the end of this time, residual UCH-L1 activity was measured with Ub-AMC at a final concentration of 100 nM.

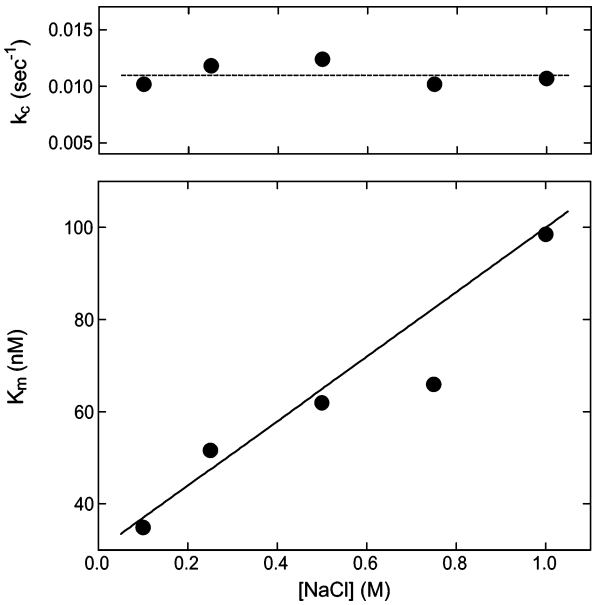

FIGURE 1: Dependence of steady-state kinetic parameters for the hydrolysis of Ub-AMC by UCH-L1 on the concentration of NaCl. At various concentrations of NaCl, values of k_c and K_m were determined from the dependence of the initial velocity on substrate Ub-AMC concentration. Reaction conditions: [UCH-L1] = 2 nM, 50 mM HEPES, 0.5 mM EDTA, 0.1 mg/mL ovalbumin, 1 mM DTT, pH 7.5, 25 °C.

RESULTS

Dependence of Kinetic Parameters on the Concentration of NaCl. In preliminary experiments, we found that K_m for the UCH-L1-catalyzed hydrolysis of Ub-AMC increased with an increase in the concentration of NaCl. These observations were confirmed in experiments in which we determined steady-state kinetic parameters for the UCH-L1-catalyzed hydrolysis of Ub-AMC, at five concentrations of NaCl that ranged from 0.1 to 1.0 M [50 mM HEPES (pH 7.5), 0.1 mg/mL ovalbumin, 0.5 mM EDTA, and 1 mM DTT at 25 °C]. At each concentration of NaCl, initial velocities were determined in duplicate at six concentrations of Ub-AMC that ranged from 3 to 120 nM. In all cases, the data could be fit to the simple Michaelis−Menten equation to provide values of k_c and K_m that are plotted as a function of NaCl concentration in Figure 1. Values of k_c were calculated from experimentally determined V_{max} values using an AMC calibration curve to convert units of FI to molarity and the nominal enzyme concentration of 2 nM. Enzyme titration with Ub-H confirmed that the nominal is equal to the actual concentration of UCH-L1 (see below). From the results depicted in Figure 1, we see that while k_c is insensitive to NaCl concentration and equal to ~0.011 s^{-1}, K_m exhibits a positive linear dependence on NaCl concentration, increasing from 35 nM at 0.1 M NaCl to 98 nM at 1 M NaCl.

pH Dependence of Steady-State Kinetic Parameters. At pH values that ranged from 5.5 to 9.5, we determined the substrate concentration dependence of initial velocities for the UCH-L1-catalyzed hydrolysis of Ub-AMC. In all cases, the data could be fit to the simple Michaelis−Menten equation and afforded the pH-dependent steady-state kinetic

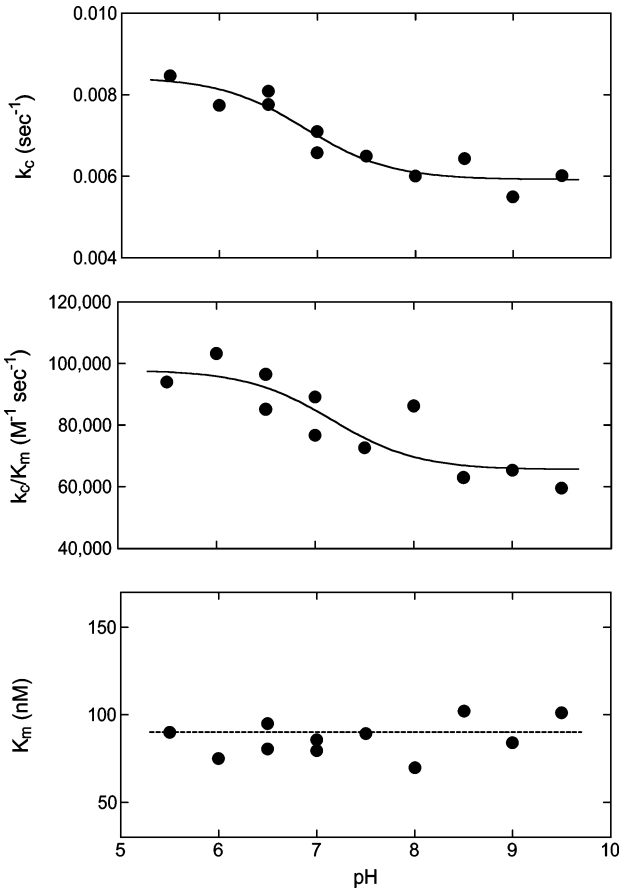

FIGURE 2: Dependence of steady-state kinetic parameters for the hydrolysis of Ub-AMC by UCH-L1 on pH. At various pH values, steady-state kinetic parameters k_c, K_m, and k_c/K_m were determined from the dependence of the initial velocity on substrate Ub-AMC concentration. Solid lines through the pH dependencies of k_c and k_c/K_m were drawn using eq 4 and best fit values summarized in the text. Reaction conditions: [UCH-L1] = 2 nM, 50 mM buffer salt, 500 mM NaCl, 0.5 mM EDTA, 0.1 ovalbumin, 1 mM DTT, 25 °C.

parameters depicted in Figure 2. Buffer crossover experiments revealed no dependence on the buffer salt.

We see that while K_m is independent of pH, both k_c and k_c/K_m show a small downward deflection at neutral pH. The data sets for the dependencies of k_c and k_c/K_m on pH could be fit to the mechanism-independent expression of eq 4:

$$k_{obs} = \frac{k_1}{1 + \frac{K_a}{[H^+]}} + \frac{k_2}{1 + \frac{[H^+]}{K_a}} \quad (4)$$

For k_c, $k_1 = (8.4 \pm 0.3) \times 10^{-3}$ s^{-1}, $k_2 = (5.9 \pm 0.2) \times 10^{-3}$ s^{-1}, and $pK_a = 6.9 \pm 0.2$, while for k_c/K_m, $k_1 = 98 \pm 6$ mM^{-1} s^{-1}, $k_2 = 65 \pm 5$ mM^{-1} s^{-1}, and $pK_a = 7.1 \pm 0.4$.

Solvent Deuterium Isotope Effects on Steady-State Kinetic Parameters. Figure 3 shows the results of an experiment in which we determined the substrate concentration dependence of initial velocities for the UCH-L1-catalyzed hydrolysis of Ub-AMC in H_2O and D_2O. These results, together with those of a repetition, are summarized in Table 1.

Reaction Progress Curves at Saturating Substrate Concentrations. In these experiments, we wanted to determine whether acylation or deacylation rate-limits k_c for the UCH-L1-catalyzed hydrolysis of Ub-AMC. If deacylation rate-limits k_c (i.e., $k_2 \gg k_3$), reaction progress curves for production of leaving group AMC (H_2N-R′ of Scheme 1) collected under the experimental condition $[S]_o \gg K_m$ will be characterized by a pre-steady-state burst that is proportional in magnitude to the concentration of UCH-L1. If on the other hand acylation rate-limits k_c (i.e., $k_2 \ll k_3$), a pre-steady-state burst will not be observed.

Typically, a phenol or an aniline is the leaving group for reactions that are catalyzed by cysteine or serine hydrolases. Given that molar extinction coefficients for these groups are on the order of 10^3-10^4 OD M^{-1} cm^{-1}, enzyme concentrations of 1−10 μM are required to reproducibly observe and precisely analyze stoichiometric bursts. Also, given that typical k_c values for cysteine and serine hydrolases are between 0.1 and 100 s^{-1}, the experiment must be done using a stopped-flow spectrophotometer. However, in this case, the leaving group is the highly fluorescent AMC moiety,

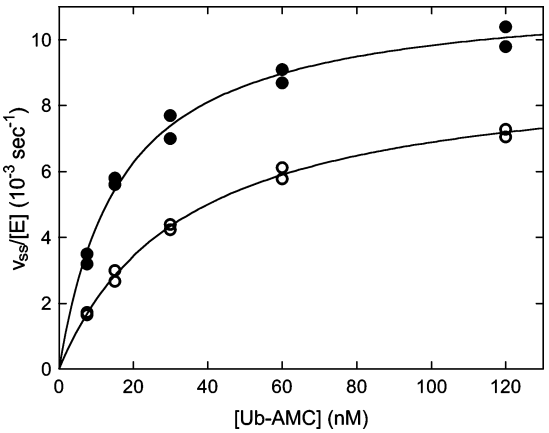

FIGURE 3: Solvent deuterium isotope effects on steady-state kinetic parameters for the hydrolysis of Ub-AMC by UCH-L1. In H_2O (○) and D_2O (●), steady-state velocities were determined as a function of Ub-AMC concentration. Solid lines were drawn using the Michaelis−Menten equation and best fit values: in H_2O, $k_c = 0.0092 \pm 0.0002$ s^{-1} and $K_m = 33.4 \pm 1.9$ nM, and in D_2O, $k_c = 0.0115 \pm 0.0003$ s^{-1} and $K_m = 16.8 \pm 1.4$ nM. Reaction conditions: [UCH-L1] = 2 nM, 50 mM HEPES, 100 mM NaCl, 0.5 mM EDTA, 0.1 mg/mL ovalbumin, 1 mM DTT, pH 7.5 and pD equivalent, 25 °C.

Table 1: Solvent Isotope Effects for UCH-L1-Catalyzed Hydrolysis of Ub-AMC[a]

		H_2O	D_2O	^Dk
experiment 1	k_c (s^{-1})	0.0103	0.0112	0.920
	K_m (nM)	33.7	18.7	1.80
	k_c/K_m (mM^{-1} s^{-1})	306	599	0.511
experiment 2	k_c (s^{-1})	0.0092	0.0115	0.800
	K_m (nM)	33.4	16.8	1.99
	k_c/K_m (mM^{-1} s^{-1})	275	685	0.401
	$^Dk_c = 0.86 \pm 0.06$			
	$^DK_m = 1.9 \pm 0.1$			
	$^D(k_c/K_m) = 0.46 \pm 0.06$			

[a] Kinetic parameters were determined from the fit to the Michaelis−Menten equation of the dependence of the reaction velocity on substrate concentration at pH 7.4 and pD equivalent (*35*) in a buffer consisting of 50 mM HEPES, 100 mM NaCl, 0.5 mM EDTA, 0.1 mg/mL ovalbumin, and 1 mM DTT at 25 °C. The enzyme concentration was 2 nM. Two independent kinetic experiments were performed in H_2O and D_2O. At the bottom of the table are shown mean isotope effects on k_c, K_m, and k_c/K_m together with values of the relative error, which was calculated using the expression $[(\sigma_H)^2 + (\sigma_D)^2]^{1/2}$, where σ is the deviation from the mean; the absolute error reported in the table is a product of the mean and the relative error.

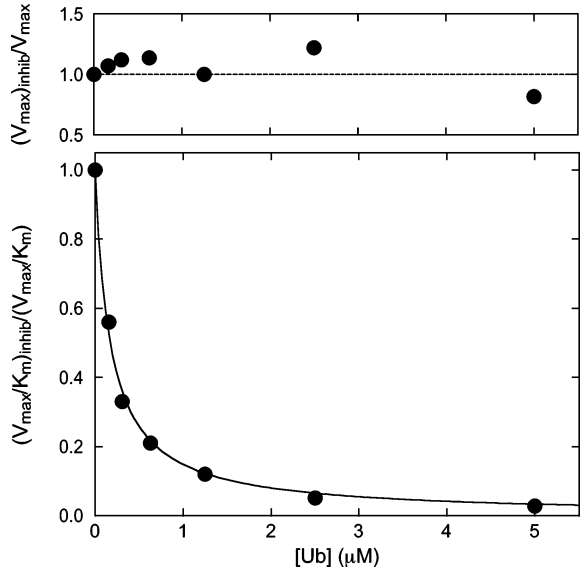

FIGURE 4: Competitive inhibition by ubiquitin of the hydrolysis of Ub-AMC by UCH-L1. As a function of Ub concentration, values of V_{max} and V_{max}/K_m were determined from the dependence of initial velocity on substrate Ub-AMC concentration. These values, relative to the value at [Ub] = 0, are plotted here as a function of Ub concentration. Lines through the data were drawn as described in the text. Reaction conditions: [UCH-L1] = 2 nM, 50 mM HEPES, 100 mM NaCl, 0.5 mM EDTA, 0.1 mg/mL ovalbumin, 1 mM DTT, pH 7.5, 25 °C.

which allowed us to use enzyme concentrations as low as 5 nM. Furthermore, since k_c for the hydrolysis of Ub-AMC by UCH-L1 is ~0.01 s^{-1}, a rapid kinetics apparatus was unnecessary and the experiment could be conducted on a conventional fluorometer.

Progress curves collected at $10K_m$ [350 nM Ub-AMC, 50 mM HEPES, 100 mM NaCl (pH 7.4), 0.5 mM EDTA, 0.1 ovalbumin, and 1 mM DTT (pH 7.4)] and at UCH-L1 concentrations of 5, 10, and 20 nM showed no hint of a burst (data not show). In these experiments, continuous stirring of reaction solutions allowed us to add enzyme without having to remove the cuvette. This reduced the dead time of the experiments to ~5 s and eliminated the possibility of missing the production of a burst. Progress curves extrapolated to zero fluorescence at t_0 and steady-state velocities were linearly dependent on enzyme concentration. Thus, it appears that $k_2 \ll k_3$ for the UCH-L1-catalyzed hydrolysis of Ub-AMC and acylation rate-limits k_c.

Mechanism of Inhibition of UCH-L1 by Ubiquitin. It was of some interest to determine if ubiquitin inhibits UCH-L1 and, if it does, by what mechanism. To this end, we determined the substrate concentration dependence for the UCH-L1-catalyzed hydrolysis of Ub-AMC at several concentrations of Ub. All data sets could be fit to the Michaelis−Menten equation to afford estimates of steady-state kinetic constants that were normalized and then plotted in Figure 4 as a function of Ub concentration. While V_{max} is independent of Ub concentration, values of V_{max}/K_m decrease as the Ub concentration increases, indicating that Ub is a competitive inhibitor of UCH-L1. The dependence of V_{max}/K_m on Ub concentration can be fit to a simple inhibition function to provide a K_i of 0.14 ± 0.01 μM.

Temperature Dependence of UCH-L1 Catalysis and Inhibition. As a function of temperature, values of k_c (=k_2) and K_m (=K_s) for the UCH-L1-catalyzed hydrolysis of Ub-AMC were determined from plots of initial velocity versus substrate concentration. This experiment was conducted at two different pH values (6.0 and 9.0).

Transition-state theory provides the basis for our analysis of the temperature dependence of k_2. According to TST, first-order rate constants for unimolecular processes have the following dependence on temperature

$$k = \kappa \frac{k_B T}{h} \exp\left(-\frac{\Delta G^{\ddagger}}{RT}\right) \quad (5)$$

where $\Delta G^{\ddagger}$, κ, k_B, h, and R are the Gibbs free energy of activation, the transmission coefficient, and the Boltzmann, Planck, and gas constants, respectively. The expression of eq 5 can be recast in quasi-thermodynamic form as eq 6

$$k = \frac{k_B T}{h} \exp\left[-\left(\frac{\Delta H^{\ddagger}}{RT} - \frac{\Delta S^{\ddagger}}{R}\right)\right] \quad (6)$$

where $\Delta H^{\ddagger}$ and $\Delta S^{\ddagger}$ are the enthalpy and entropy of activation, respectively. In this equation, the transmission coefficient is assumed to be equal to 1. Finally, eq 6 can be rearranged to eq 7:

$$\ln\left[k\left(\frac{h}{k_B T}\right)\right] = -\frac{\Delta H^{\ddagger}}{RT} + \frac{\Delta S^{\ddagger}}{R} \quad (7)$$

Equation 7 predicts that a plot of $\ln[k(h/k_BT)]$ versus inverse temperature (i.e., an Eyring plot) will be linear with a slope and an intercept proportional to $\Delta H^{\ddagger}$ and $\Delta S^{\ddagger}$, respectively.

The results of the experiment at pH 6 are shown in the top panel of Figure 5. Best fit values according to eq 7, and those for pH 9, are summarized in Table 2.

To analyze the temperature dependence of the K_s values that we determined in these experiments, we first calculated their reciprocals to transform them into association constants, K_{assoc}. We then multiplied them by a standard-state concentration of 10^{-6} M to yield unitless equilibrium constants, K_{assoc}'. These latter values were then used to construct van't Hoff plots of $\ln[K_{assoc}']$ versus inverse temperature.

For simple mechanisms, van't Hoff plots are linear and obey eq 8.

$$\ln[K_{assoc}'] = -\frac{\Delta H_{assoc}}{RT} + \frac{\Delta S_{assoc}}{R} \quad (8)$$

However, in this case, curvature is observed, as can be seen in the bottom panel of Figure 5. Such curvature in a van't Hoff plot is consistent with an association mechanism having a negative change in heat capacity. The applicable thermodynamic equation is shown in eq 9

$$\ln[K_{assoc}'] = -\frac{\Delta H}{RT} + \frac{\Delta S}{R} + \frac{\Delta C_p}{R}\left[-1 + \frac{T_{ref}}{T} + \ln\left(\frac{T}{T_{ref}}\right)\right] \quad (9)$$

to which the data of Figure 5 could be successfully fit. Best fit values are summarized in Table 2 and were used to draw the line through the data in the figure.

The temperature dependence of K_i, for the inhibition of UCH-L1 by Ub, was also determined. As a function of temperature, values of $K_{i,app}$ were determined from the

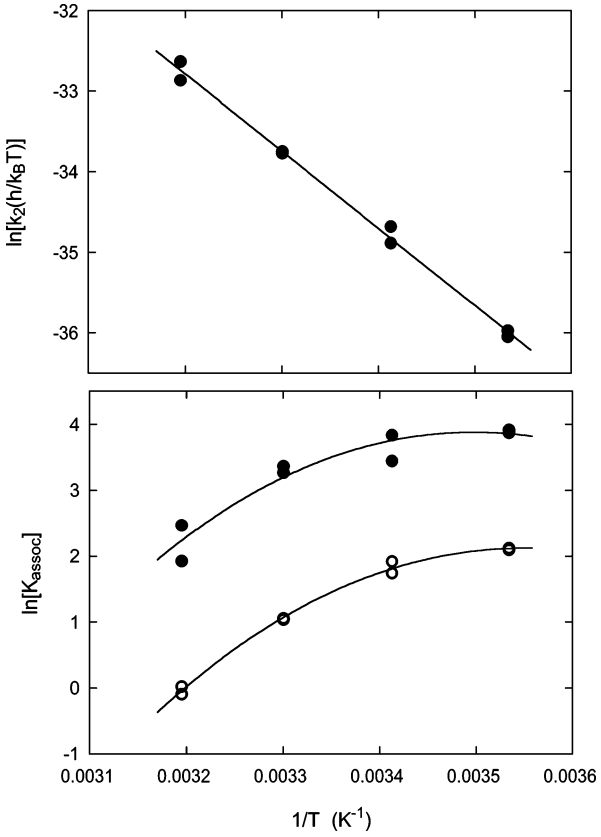

FIGURE 5: Temperature dependencies for the UCH-L1-catalyzed hydrolysis of Ub-AMC and for the inhibition of UCH-L1 by Ub. The top panel contains the Eyring plot for k_2. Data were fit to eq 7, and the line was drawn using the best fit values summarized in Table 2. The bottom panel contains van't Hoff plots for K_s, for Ub-AMC hydrolysis (●), and K_i, for inhibition by Ub (○). These data sets were fit to eq 9 and the lines drawn using the best fit values of Table 2. Reaction conditions: [UCH-L1] = 4 nM, 50 mM HEPES, 100 mM NaCl, 0.5 mM EDTA, 0.1 mg/mL ovalbumin, 1 mM DTT, pH 6.0.

Table 2: Temperature Dependencies of UCH-L1 Catalysis and Inhibition[a]

		acylation		association		
reactant	pH	$\Delta H^{\ddagger}$	$-T\Delta S^{\ddagger}$	ΔH	$-T\Delta$ '	$-T\Delta C_p$
Ub-AMC	6.0	19.1 ± 0.5	1.4 ± 0.5	−14 ± 2	12 ± 2	240 ± 80
Ub-AMC	9.0	20.3 ± 0.8	0.1 ± 0.8	−14 ± 2	13 ± 2	310 ± 95
Ub	6.0	−	−	−17 ± 1	16 ± 1	240 ± 30

[a] Reaction conditions: [UCH-L1] = 4 nM, 50 mM buffer salt, 100 mM NaCl, 0.5 mM EDTA, 0.1 ovalbumin, 1 mM DTT. Units: kilocalories per mole for $\Delta H^{\ddagger}$, ΔH, $-T\Delta S^{\ddagger}$, $-T\Delta S$, and $-T\Delta C_p$ at 303 K.

dependence of velocity on Ub concentration at a single substrate concentration of 20 nM. Values of K_i were then calculated by dividing $K_{i,app}$ by $(1 + [S]/K_m)$, using the temperature-dependent K_m values that were determined above. To analyze the temperature dependence of these K_i values, a method identical to that employed for K_s was used. van't Hoff plots for K_i were also curved and could be fit to eq 9. Results are summarized in Table 2.

Solvent Isotope Effect for the Inhibition of UCH-L1 by Ubiquitin. Initial velocities at a Ub-AMC concentration of 7.5 nM were determined as a function of Ub concentration, in H_2O and D_2O. These curves are shown in Figure 6 and could be fit by a nonlinear least-squares method to give the

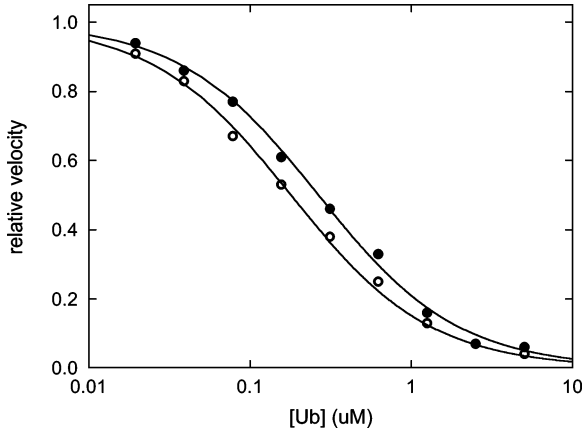

FIGURE 6: Solvent deuterium isotope effect for the inhibition of UCH-L1 by ubiquitin. Steady-state velocities were determined as a function of Ub concentration in H_2O (○) and D_2O (●). Inhibition binding curves were drawn as described in the text. Reaction conditions: [UCH-L1] = 2 nM, [Ub-AMC] = 7.5 nM, 50 mM HEPES, 100 mM NaCl, 0.5 mM EDTA, 0.1 mg/mL ovalbumin, 1 mM DTT, pH 7.5 and pD equivalent, 25 °C.

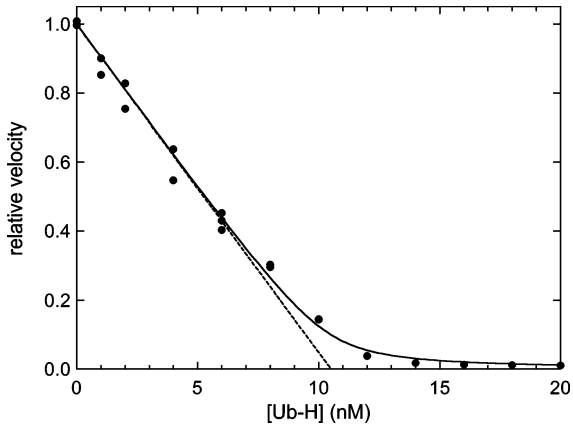

FIGURE 7: Titration of UCH-L1 by Ub-H. Enzyme, at a nominal concentration of 10 nM, was incubated with various concentrations of Ub-H for 2 h and residual activity measured after the addition of 120 nM Ub-AMC. This activity, relative to the activity at [Ub-H] = 0, is plotted here as a function of Ub-H concentration. The solid line through the data points is drawn using eq 10 and best fit parameters: $[E]_o = 11.0 \pm 0.3$ nM and $K_i = 0.10 \pm 0.06$ nM. Reaction conditions: 50 mM HEPES, 100 mM NaCl, 0.5 mM EDTA, 0.1 mg/mL ovalbumin, 1 mM DTT, pH 7.5, 25 °C.

following estimates: $(K_{i,app})_{H_2O} = 0.265 \pm 0.010$ μM and $(K_{i,app})_{D_2O} = 0.179 \pm 0.008$ μM. Given K_m values of 33 and 17 nM in H_2O and D_2O (see Table 1), respectively, and a competitive mechanism of inhibition, these apparent K_i values can be divided by the term $(1 + [S]/K_{m,L_2O})$ to provide estimates of K_i values: $(K_i)_{H_2O} = 0.22$ μM and $(K_i)_{D_2O} = 0.12$ μM. This allows us to calculate a solvent isotope effect on K_i of approximately 1.8. Given the error limits associated with the K_i determinations as well as with the determination of K_m values, we believe that this isotope effect has a relative error on the order of 10%.

Titration of UCH-L1 with Ub-H. Preliminary experiments suggested that Ub-H is a potent inhibitor of UCH-L1 with a K_i value of <1 nM. To confirm this finding, we conducted an experiment in which residual enzymatic activity, after a 2 h incubation of enzyme and inhibitor, was measured for reaction solutions in which $[I]_o \sim [E]_o > K_i$ (see Figure 7). Fitting the data to eq 10, the expression for tight binding inhibition

$$\frac{v_{\text{inhib}}}{v_{\text{control}}} = \frac{1}{2[\text{E}]_o}[[\text{E}]_o - [\text{I}]_o - K_i + \sqrt{([\text{I}]_o + K_i - [\text{E}]_o)^2 + 4K_i[\text{E}]_o}] \quad (10)$$

provides estimates of K_i and $[E]_o$, the concentration of catalytically active enzyme: $K_i = 0.10 \pm 0.06$ nM and $[E]_o = 11.0 \pm 0.3$ nM. This experiment not only tells us that Ub-H is a very potent inhibitor of UCH-L1 but also confirms the enzyme concentration.

Time-Dependent Inhibition and Solvent Isotope Effects for the Association of Ub-H with UCH-L1. In the course of these studies, we found that Ub-H is a slow binding inhibitor of UCH-L1. Values of k_{obs}, the pseudo-first-order rate constant for the approach to steady state, were determined as a function of Ub-H concentration in H_2O and D_2O (see Figure 8) as previously described for the inhibition of UCH-L3 and isopeptidase T by Ub-H (*6*, *7*). Equation 11 expresses the dependence of k_{obs} on Ub-H concentration

$$k_{obs} = k_{on}\left(1 + \frac{[S]}{K_m}\right)[I] + k_{off} \quad (11)$$

where k_{on} is the second-order rate constant for association of the enzyme and inhibitor and k_{off} is the first-order rate constant for dissociation of the resultant E−I complex.

The slopes of these lines are 238 and 182 mM^{-1} s^{-1} in H_2O and D_2O, respectively. Using eq 11, a substrate concentration of 15 nM, and the appropriate K_m values (i.e., $K_{m,H_2O} = 33$ nM and $K_{m,D_2O} = 17$ nM; see Table 1), we can calculate k_{on} values of 346 and 326 mM^{-1} s^{-1} in H_2O and D_2O, respectively, and an isotope effect ($^Dk_{on} = k_{on,H_2O}/k_{on,D_2O}$) of 1.06. In a repeat of this experiment (data not shown), an isotope effect of 0.96 was found. Thus, we can calculate a $^Dk_{on}$ of 1.01 ± 0.05.

In both solvents, the *y*-axis intersection is zero within experimental error. From this result, we can estimate the conservative limit: $k_{off} \leq 5 \times 10^{-5}$ s^{-1}. This allows us to calculate a K_i of ≤0.1 nM, in agreement with the titration data (see above).

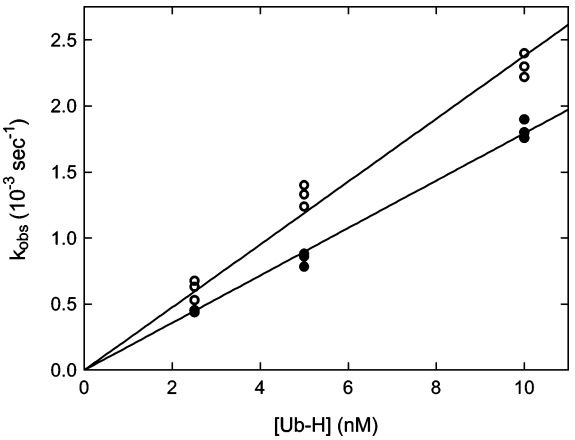

FIGURE 8: Solvent deuterium isotope effect for the association of UCH-L1 with Ub-H. Values of k_{obs}, for the association of UCH-L1 with Ub-H, were determined in H_2O (○) and D_2O (●) as described in the text. Slopes of the linear dependencies of k_{obs} on [Ub-H] are 238 ± 59 and 182 ± 42 mM^{-1} s^{-1} in H_2O and D_2O, respectively, and were used to calculate values of k_{on} as described in the text. [UCH-L1] = 1 nM, [Ub-AMC] = 15 nM, 50 mM HEPES, 100 mM NaCl, 0.5 mM EDTA, 0.1 mg/mL ovalbumin, 1 mM DTT, pH 7.5 and pD equivalent, 25 °C.

Scheme 2: Chemical Mechanism for Cysteine Hydrolases

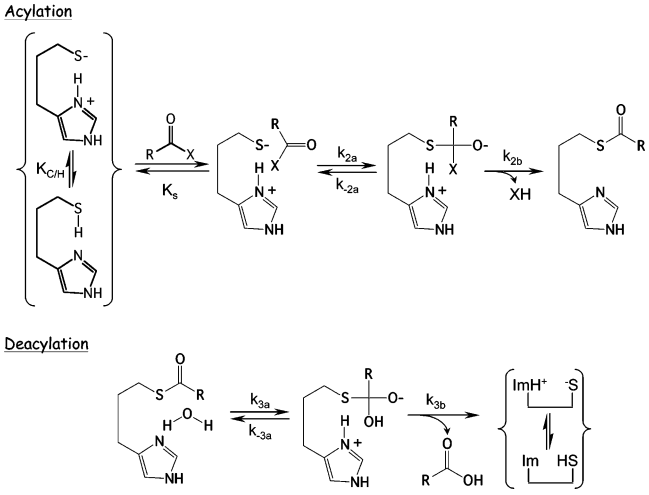

DISCUSSION

In this section, we discuss results of our mechanistic studies of the three reactions of UCH-L1 that we characterized for this paper: hydrolysis of Ub-AMC, inhibition by Ub, and slow, tight binding inhibition by Ub-H. After first providing the mechanistic backdrop for these discussions, we consider general aspects of UCH-L1 kinetics and mechanism and then analyze the temperature dependencies and solvent deuterium isotope effects that we measured.

Chemical Mechanism of Cysteine Hydrolases and the Anomalous Active Site of UCH-L1. A key feature of the chemical mechanism of cysteine hydrolases (see Scheme 2) is the existence of a catalytically crucial Cys/His diad. The Cys/His diad of free enzyme exists as two tautomers, Cys-SH/His-Im and Cys-S^-/His-ImH^+, whose equilibrium is governed by $K_{C/H}$ (=[SH/Im]/[S^-/ImH^+]). In the acylation manifold of this mechanism, the first step is formation of the Michaelis complex, S^-/ImH^+:R-C(O)X, which can occur by either of two routes: (i) direct binding of substrate to S^-/ImH^+ or (ii) binding of substrate to SH/Im followed by rapid proton transfer to form S^-/ImH^+:R-C(O)X. Formation of the tetrahedral intermediate is thought to occur by nucleophilic attack of the thiolate anion on the carbonyl carbon of the substrate with no catalytic assistance by general acids or bases (*14*). In the final step of acylation, the tetrahedral intermediate collapses to form the acyl-enzyme intermediate with expulsion of leaving group XH. For amine leaving groups, this step is thought to be subject to general acid catalysis by the imidazolium cation of the active site His.

Deacylation involves attack of water on the acyl-enzyme intermediate to form a tetrahedral intermediate which then collapses to produce a second product and liberate free enzyme. While formation of the tetrahedral intermediate is thought to involve general base catalysis by the active site His, breakdown of the intermediate with expulsion of a thiolate anion should not require protolytic catalysis.

While UCH-L1 is a member of the family of cysteine hydrolases, it possesses a unique structural feature that sets it apart from other enzymes of this family. X-ray crystallographic studies have revealed that in the active site of UCH-L1 there is a water molecule situated between Cys[90]

Scheme 3: Acylation of UCH-L1

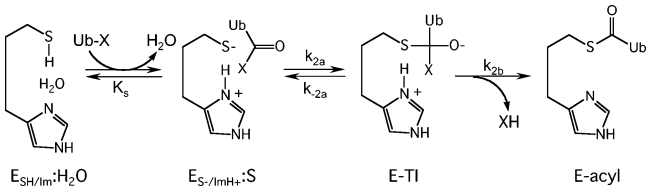

and His[161], the residues that comprise the enzyme's catalytic Cys/His diad (*15*). The distance between the imidazole ring of His[161] and the water molecule is 4.9 Å, while the distance between the water and the sulfur atom of Cys[90] is 3.9 Å. Both of these distances are likely too long to allow the water molecule to serve as either a proton shuttle or general catalyst during substrate turnover. Thus, we believe that it must be ejected from the site to allow a conformational change that would bring Cys[90] and His[161] sufficiently close to form a catalytically competent Cys/His diad. Interestingly, a similar distance of 9.7 Å exists between catalytic His[464] and Cys[223] residues of HAUSP, a mechanistically related UBP enzyme (*16*). It was hypothesized that after binding of substrate, a conformational change of the enzyme occurs to bring His[464] and Cys[223] sufficiently close to form an effective catalytic diad.

The mechanism we propose for acylation of UCH-L1 is shown in Scheme 3. The key feature that distinguishes it from the acylation mechanism of Scheme 2 is the structure of reactant-state UCH-L1, which is shown to have a water at its active site. In this mechanism, the substrate dissociation constant K_s must be a complex composite that governs four processes: (i) binding of substrate to enzyme, (ii) expulsion of water from the active site, (iii) conformational isomerization to bring Cys[90] and His[161] within hydrogen bonding distance, and (iv) tautomerization to produce the catalytically competent $E_{S^-/ImH^+}-S$ species. At this time, we do not know the order in which these processes occur. Furthermore, while we assume that these process are in rapid equilibrium, it is of course possible that one of these processes is slow relative to the chemistry of acylation and would therefore contribute to limiting the rate of substrate turnover. Clearly then, the mechanistic proposal of Scheme 3, and perhaps details of the interpretation of our mechanistic studies that follow, may well have to be modified as more data concerning these processes become available.

General Aspects of Reactions of UCH-L1. The hydrolysis of Ub-AMC by UCH-L1 follows simple Michaelis−Menten kinetics under all conditions we studied. We found that while the enzyme binds substrate with high affinity (i.e., $K_m \sim 50$ nM), it affects hydrolytic turnover with notable inefficiency. k_c is on the order of 0.01 s^{-1}, a very slow reaction by most any enzymatic measure. The comparisons in Table 3 illustrate this point. We see in this table that k_c is nearly 10^3 times greater for UCH-L3, a close homologue of UCH-L1. K_m values are identical for the two enzymes.

The absence of a pre-steady-state burst of AMC release during turnover of saturating concentrations of Ub-AMC indicates that k_c is rate-limited by acylation. Thus, $k_2 \ll k_3$, thereby allowing eqs 2 and 3 to be simplified to $k_c = k_2$ and $K_m = K_s$, respectively. These simplifications will allow a more conclusive interpretation of our temperature dependencies and isotope effects where K_m can be said to correspond to a true equilibrium constant K_s and k_c can be said to correspond to acylation alone.

Table 3: Kinetic Parameters for Hydrolysis of Ub-AMC by UCH-L1 and UCH-L3

	UCH-L1	UCH-L3[c]	k_{UCH-L3}/k_{UCH-L1}
k_c[a] (s^{-1})	0.01	8.1	810
K_m[a] (nM)	35	39	1
k_c/K_m[a] (μM^{-1} s^{-1})	0.29	210	720
k_{on}[b] (μM^{-1} s^{-1})	0.33	35	110

[a] Hydrolysis of Ub-AMC, in 50 mM HEPES, 100 mM NaCl, 0.5 mM EDTA, 0.1 mg/mL ovalbumin, and 1 mM DTT at pH 7.5 and 25 °C. [b] Association with Ub-H, in 50 mM HEPES, 100 mM NaCl, 0.5 mM EDTA, 0.1 mg/mL ovalbumin, and 1 mM DTT in 25 °C. [c] These results are from a literature report under the following reaction conditions: 50 mM HEPES, 0.5 mM EDTA, 0.1 mg/mL ovalbumin, 1 mM DTT, pH 7.5, 25 °C (*7*).

Steady-state kinetic parameters k_c and k_c/K_m for hydrolysis of Ub-AMC by UCH-L1 are largely pH-independent in the pH range that was explored in these studies (i.e., 5.5−9.5), indicating that catalytically essential ionizations must have pK_a values that fall outside of this range. For papain and other cysteine proteases, bell-shaped dependencies of k_c/K_m on pH are ordinarily observed, with pK_a values of 3.5−4.0 and 8.4−9.5 (*17*−*20*). The low pK_a of 4 is thought to correspond to dissociation of inactive SH/ImH^+ to form catalytically active S^-/ImH^+, while the high pK_a of 9 is thought to correspond to ionization of S^-/ImH^+ to form inactive S^-/Im. If the pH dependence for UCH-L1 catalysis is similar to that of other cysteine hydrolases, then the narrow pH range that we used in these experiments would have precluded us from observing the low pK_a and possibly the high pK_a, if it was perturbed to a value of ≥10. While other mechanisms, such as a pH-independent rate-limiting step, can be posited to explain the lack of an observable pH dependence for UCH-L1 catalysis, there are currently no data to warrant proposition of such hypotheses.

The C-terminal aldehyde of ubiquitin is a potent inhibitor of UCH-L1 with a K_i value that is less than 0.1 nM. Ub-H is known to form a hemithioacetal with the active site Cys residues of the UCH enzyme Yuh1 and the UBP enzyme HAUSP (*16*, *21*) and likely does so with UCH-L1. In all cases, the potency of inhibition of deubiquitinating enzymes by Ub-H is extreme and is thought to originate from the resemblance of the hemithioacetal to the transition state for acylation (*7*).

Temperature Dependence of UCH-L1 Catalysis and Inhibition. We studied the temperature dependence of UCH-L1 at pH 6.0 and 9.0, values that reflect the plateaus of the pH dependence for this enzyme. In doing this, we were exploring the possibility that the two plateaus represent two different catalytic processes which might manifest different activation or thermodynamic parameters. As evidenced in the results given in Table 2, the temperature dependencies at these pH values are nearly identical, strongly suggesting the plateaus do not originate from any mechanistically significant difference in the catalytic mechanism.

The Eyring plots for acylation are linear, indicating that, over the temperature range of this experiment, the rate-limiting step has not changed. Interestingly, the entire free energy of activation is manifested in the enthalpy term; the entropy of activation is essentially equal to zero. This

Scheme 4: Origins of Solvent Deuterium Isotope Effects

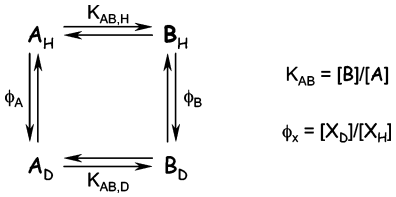

indicates that when the reaction proceeds from the reactant state of k_2 (i.e., the Michaelis complex) to the rate-limiting transition state, little or no reorganization occurs at the active site, suggesting a "preorganization" mechanism (*22*) in which the Michaelis complex substrate and active site residues are oriented for optimal catalytic interaction.

Unlike the Eyring plots for k_2, the van't Hoff plots for both K_s, for Ub-AMC hydrolysis, and K_i, for Ub inhibition, are concave. These data can be fit to the thermodynamic expression of eq 9, which includes a mechanism-independent term for a change in heat capacity, to yield large, negative values of ΔC_p on the order of -0.8 kcal mol^{-1} deg^{-1}. There are a number of ways to interpret such values for the association of proteins with ligands (*23*−*26*). Negative values of ΔC_p can reflect the decrease in solvent accessible surface area that occurs upon the binding of a ligand to a protein. Alternatively, these values can indicate a mechanism for ligand binding in which association is coupled to a conformational isomerization of the protein (*24*, *25*). And, of course, $-\Delta C_p$ can result from a combination of both these reasons. Currently, we have insufficient information to make an informed decision about which of these mechanisms is at work and how they might relate to the water molecule at the active site of UCH-L1.

Solvent Deuterium Isotope Effects for Catalysis by UCH-L1. To explore the hydrolytic reaction in more detail, we determined solvent deuterium isotope effects (see Table 1) and found the following: $^{D}k_c = {}^{D}k_2 = 0.86 \pm 0.06$, $^{D}K_m = {}^{D}K_s = 1.9 \pm 0.1$, and $^{D}(k_c/K_m) = {}^{D}(k_2/K_s) = 0.46 \pm 0.06$. The solvent isotope effect that we observe on k_c/K_m is similar in magnitude to $^{D}(k_c/K_m)$ values for other Cys/His diad hydrolases and acyltransferases (*27*−*34*). These values range from inverse effects of ~0.4 to slightly normal effects of 1.1. However, in contrast to the inverse isotope effect on $^{D}k_c$ that we observe for the reaction of UCH-L1, literature values are usually large and normal, ranging from 1.5 to 3.5, indicating protolytic catalysis, probably by His, for these reactions.

Our interpretation of the solvent isotope effects for reactions of UCH-L1 starts with a discussion of how solvent isotope effects are related to hydrogen fractionation factors. Consider Scheme 4 in which we depict the multiple equilibria for the chemical interconversion of molecular species A and B, where A and B each have a single exchangeable proton.

The solvent deuterium isotope effect on the equilibrium constant K_{AB} can be expressed in eq 12 as the ratio of hydrogen fractionation factors ϕ_A and ϕ_B (*35*) for the two species that are in equilibrium.

$$^{D}K_{AB} = \frac{K_{AB,H}}{K_{AB,D}} = \frac{\phi_A}{\phi_B} \tag{12}$$

If A and B have several exchangeable hydrogenic sites, eq 12 becomes

$$^{D}K_{AB} = \frac{\prod_i \phi_{A,i}}{\prod_j \phi_{B,j}} \tag{13}$$

where i and j are the number of exchangeable hydrogenic sites on A and B, respectively.

Likewise, solvent deuterium isotope effects on rate constants can be expressed as

$$^{D}k = \frac{\prod_i \phi_{r,i}}{\prod_j \phi_{\ddagger,j}} \tag{14}$$

where $\phi_{r,i}$ and $\phi_{\ddagger,j}$ are fractionation factors for the exchangeable hydrogens in the reactant state and transition state, respectively.

The solvent isotope effects that we observed for UCH-L1 are all for the acylation manifold and thus are functions of isotope effects on the microscopic rate constants of the mechanism of Scheme 3: $^{D}K_s$, $^{D}k_{2a}$, $^{D}k_{-2a}$, and $^{D}k_{2b}$. One way to proceed is to first consider the magnitudes of each of these individual isotope effects.

According to the mechanism of Scheme 3, UCH-L1 likely possesses only two exchangeable hydrogenic sites with nonunity fractionation factors: the thiol moiety of the active site Cys residue in the $E_{SH/Im}-H_2O$ complex and the protonic bridge that forms between the imidazolium of His^{161} and the departing amine leaving group of the transition state of the general acid-catalyzed decomposition of the E−TI tetrahedral intermediate. The fractionation factor for the thiol hydrogen is 0.4, while values for the protonic bridges formed during protolytic catalysis can range from 0.6 to 0.2, with a typical average value of ~0.3 (*35*). Given this, we can assign the following rough estimates to the solvent isotope effects for the five discrete reaction steps of Scheme 3:

$$^{D}K_s = \phi_{S^-/ImH^+-S}/\phi_{SH/Im} = 1/0.4 = 2.5 \tag{15}$$

$$^{D}k_{2a} = \phi_{E-S}/\phi_{\ddagger,2a} = 1 \tag{16}$$

$$^{D}k_{-2a} = \phi_{TI}/\phi_{\ddagger,-2a} = 1 \tag{17}$$

$$^{D}k_{2b} = \phi_{TI}/\phi_{\ddagger,2b} = 1/0.3 = 3.3 \tag{18}$$

With these estimates of isotope effects on individual reactions, it is possible to calculate estimates of the overall isotope effects on K_m, k_c, and k_c/K_m.

The observed solvent isotope effect on K_m of 1.9 and the solvent isotope effect on K_i of 1.8 for inhibition by Ub suggest mechanisms in which the ground-state enzyme exists predominantly as SH/Im, and the E−S and E−I complexes that form have tautomerized to S^-/ImH^+. The agreement between the observed values with the predicted value of ~2.5 supports the veracity of the mechanism of Scheme 3.

Turning now to k_c, we see from Scheme 3 that this kinetic constant will have the form shown in eq 19

$$k_c = \frac{k_{2a}k_{2b}}{k_{-2a} + k_{2b}} \quad (19)$$

There are two limiting conditions that we need to consider. If $k_{-2a} \ll k_{2b}$, then $k_c = k_{2a}$ and ${}^{D}k_c = Dk_{2a}$, which has a value of approximately 1. On the other hand, if $k_{-2a} \gg k_{2b}$, then $k_c = (k_{2a}/k_{-2a})k_{2b}$ and ${}^{D}k_c = ({}^{D}k_{2a}/{}^{D}k_{-2a}){}^{D}k_{2b}$, which has a value of ~3. Since the observed isotope effect on k_c is 0.86, we can conclude that $k_{-2a} \ll k_{2b}$ and formation of the tetrahedral intermediate rate-limits acylation. The fact that the observed isotope effect is not precisely 1 but rather is slightly inverse may suggest, in addition, that the Cys/His diad exists in the E−S complex partially as the SH/Im neutral species and not entirely as the S^-/ImH^+ ion pair. This would also explain why ${}^{D}K_m$ and ${}^{D}K_i$ are not as large as the theoretical limit of 2.5.

From the analysis given above, we can see that k_c/K_m equals k_{2a}/K_s. Thus, it is clear that the observed isotope effect on k_c/K_m of 0.46 is equivalent to ${}^{D}(k_{2a})/{}^{D}(K_s)$ and results from a mechanism in which that the Cys/His diad of UCH-L1 exists predominantly as the neutral SH/Im species and that acylation is rate-limited by attack of the thiolate on the carbonyl carbon of the N-terminal Gly of Ub-AMC.

Solvent Deuterium Isotope Effect for Association of UCH-L1 with Ub-H. The solvent isotope effect on k_{on} for the inhibition of UCH-L1 by Ub-H is 1.01 ± 0.05. Our analysis of this effect begins with eq 14, where we see that the isotope effect is the ratio of products of reactant-state and transition-state fractionation factors.

In the reactant state, there are three protonic sites that we need to consider. One of these is the sulfhydryl group of the free enzyme with its fractionation factor of 0.4−0.5. The other two sites correspond to the hydroxyls of the hydrated aldehyde functionality of Ub-H. Since the hydrate is the stable form of the aldehyde in aqueous solution [i.e., K_{hyd}-$[H_2O]$ = [hydrate]/[aldehyde] ~ 10 (*36*)], it corresponds to the reactant state of the inhibitor that we need to consider here. The product of fractionation factors for the two protonic sites has been measured for a number of aldehydes and equals unity (*37*). Thus, the overall product of the three reactant-state fractionation factors lies between 0.4 and 0.5. Given an isotope effect of 1.0, this means that the product of fractionation factors for the transition state must be in the range of 0.4−0.5, or 0.45 ± 0.05. A fractionation factor of 0.45 corresponds to an isotope effect of 2.2, which is in the range of isotope effects observed for reactions that are subject to protolytic catalysis and suggests that formation of the hemithioacetal between UCH-L1 and Ub-H may be subject to general base catalysis by the imidazole of the active site His residue.

This mechanistic proposal for the association of UCH-L1 and Ub-H stands in contrast to the mechanism we proposed for tetrahedral intermediate formation between UCH-L1 and Ub-AMC, which involved direct attack of thiolate anion with no general catalysis. Combined, these findings suggest that UCH-L1 possesses a certain mechanistic plasticity. This is illustrated in Scheme 5 where the two principal mechanistic alternatives are shown. We see that if X is AMC the upper pathway involving direct attack is followed, while if X is H the lower pathway involving general catalysis is followed.

In the future, we will extend these studies to other leaving groups, to see which mechanism of Scheme 5 is followed, and to investigations of deacylation, which was not addressed at all here. Finally, we will use these insights to help in our design and optimization of inhibitors of UCH-L1.

Scheme 5: Alternative Mechanisms for Tetrahedral Adduct Formation for Reactions of UCH-L1

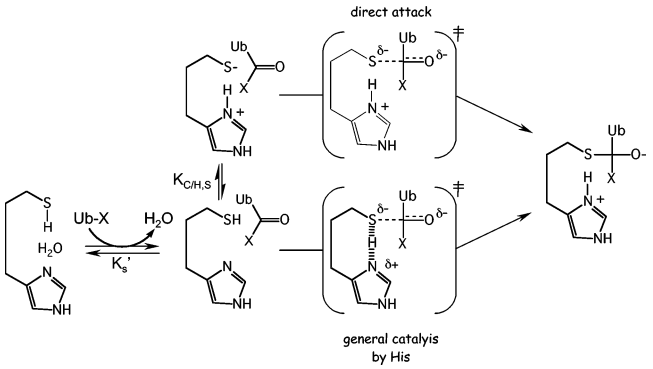

REFERENCES

1. Wilkinson, K. D. (2000) Ubiquitination and Deubiquitination: Targeting of Proteins for Degradation by the Proteasome, *Cell Dev. Biol. 11*, 141−148.
2. Kim, J. H., Park, K. C., Chung, S. S., Bang, O., and Chung, C. H. (2003) Deubiquitinating Enzymes as Cellular Regulators, *J. Biochem. 134*, 9−18.
3. Sing, S. S. (2003) Deubiquitinating Enzymes: The Importance of Driving in Reverse Along the Ubiquitin-Proteasome Pathway, *Int. J. Biochem. Cell Biol. 35*, 590−605.
4. Amerik, A. Y., and Hochstrasser, M. (2004) Mechanism and Function of Deubiquitinating Enzymes, *Biochim. Biophys. Acta 1695*, 189−207.
5. Stein, R. L., Chen, Z., and Melandri, F. D. (1995) Kinetic Studies of Isopeptidase T: Modulation of Peptidase Activity by Ubiquitin, *Biochemistry 34*, 12616−12623.
6. Melandri, F. D., Grenier, L., Plamondon, L., Huskey, P., and Stein, R. L. (1996) Kinetic Mechanism of the Slow- and Tight-Binding Inhibition of Isopeptidase-T by Ubiquitin Aldehyde, *Biochemistry 35*, 12893−12900.
7. Dang, L. C., Melandri, F. D., and Stein, R. L. (1998) Kinetic and Mechanistic Studies on the Hydrolysis of Ubiquitin C-Terminal 7-Amido-4-Methylcoumarin by Deubiquitinating Enzymes, *Biochemistry 37*, 1868−1879.
8. Rohan de Silava, H., Khan, N. L., and Wood, N. W. (2000) The Genetics of Parkinson's Disease, *Curr. Opin. Genet. Dev. 10*, 292−298.
9. Chung, W. W., Dawson, V. L., and Dawson, T. M. (2001) The Role of the Ubiquitin-Proteasome Pathway in Parkinson's Disease and Other Neurodegenerative Disorders, *Trends Neurosci. 24*, S7−S14.
10. Liu, Y., Fallon, L., Lashuel, H. A., Liu, Z., and Lansbury, P. T. (2002) The UCH-L1 Gene Encodes Two Opposing Enzymatic Activities that Affect α-Synculein Degradation and Parkinson's Disease Susceptibility, *Cell 111*, 209−218.
11. al-Katib, A. M., Mohammad, R. M., Maki, A., and Smith, M. R. (1995) Induced Expression of a Ubiquitin C-Terminal Hydrolase in Acute Lymphoblastic Leukemia, *Cell Growth Differ. 6*, 211−217.
12. Caballero, O. L., Resto, V., Patturagan, M., Meerzaman, D., Gou, M. Z., Engles, J., Yochem, R., Ratovitski, E., Sidransky, D., and Jen, J. (2002) Interaction and Colocalization of PGP9.5 with JAB1 and p27(Kip1), *Oncogene 21*, 3003−3010.
13. Liu, Y., Lashuel, H. A., Choi, S., Xing, X., Case, A., Ni, J., Yeh, L.-A., Cuny, G. D., Stein, R. L., and Lansbury, P. T. (2003) Discovery of Inhibitors That Elucidate the Role of UCH-L1 Activity in the H1299 Lung Cancer Cell Line, *Chem. Biol. 10*, 837−846.
14. Fersht, A. R. (1999) in *Structure and Mechanisms in Protein Science: A Guide to Enzyme Catalysis and Protein Folding*, pp 413−416, W. H. Freeman and Co., New York.
15. Das, C., Hoang, Q. Q., Kreinbring, C. A., Luchansky, S. J., Meray, R. K., Ray, S. S., Lansbury, P. T., Ringe, D., and Petsko, G. A. (2006) Structural Basis for Conformational Plasticity of the

Parkinson's Disease-Associated Ubiquitin Hydrolase UCH-L1, *Cell* (submitted for publication).
16. Hu, M., Li, P., Li, M., Li, W., Yao, T., Wu, J.-W., Gu, W., Cohen, R. E., and Shi, Y. (2002) Crystal Structure of UBP-Family Deubiquitinating Enzyme and in Complex with Ubiquitin Aldehyde, *Cell 111*, 1041−1054.
17. Shipton, M., and Brocklehurst, K. (1978) Characterization of the Papain Active Centre by Using Two-Protonic-State Electophiles as Reactivity Probes, *Biochem. J. 171*, 385−401.
18. Polgar, L. (1974) Mercaptide-Imidazolium Ion-Pair: The Reactive Nucleophile in Papain Catalysis, *FEBS Lett. 47*, 15−18.
19. Lowe, G. (1976) The Cysteine Proteases, *Tetrahedron 32*, 291−302.
20. Sarkany, Z., Shern, T., and Polgar, L. (2000) Characterization of the Active Site Thiol Group of Rhinovirus 2A Proteinase, *FEBS Lett. 481*, 289−292.
21. Johnston, S. C., Riddle, S. M., Cohen, R. E., and Hill, C. P. (1999) Structural Basis for the Specificity of Ubiquitin C-Terminal Hydrolases, *EMBO J. 18*, 3877−3887.
22. Rajagopalan, P. T. R., and Benkovic, S. (2002) Preorganization and Protein Dynamics in Enzyme Catalysis, *Chem. Rec. 2*, 24−36.
23. Sturtevant, J. M. (1977) Heat Capacity and Entropy Changes in Processes Involving Proteins, *Proc. Natl. Acad. Sci. U.S.A. 74*, 2236−2240.
24. Eftink, M. R., Anusiem, A. C., and Biltonen, R. (1983) Enthalphy-Entropy Compensation and Heat Capacity Changes for Protein−Ligand Interactions: General Thermodynamics Models and Data for the Binding of Nucleotides to Ribonuclease A, *Biochemistry 22*, 3884−3896.
25. Eftink, M. R., and Biltonen, R. (1983) Energetics of Ribonuclease A Catalysis. 3. Temperature Dependence of the Hydrolysis of Cytidine Cyclic 2′,3′-Phosphate, *Biochemistry 22*, 5140−5150.
26. Prabhu, N. V., and Sharp, K. A. (2005) Heat Capacity in Proteins, *Annu. Rev. Phys. Chem. 56*, 521−548.
27. Whitaker, J. R., and Bender, M. L. (1965) Kinetics of Papain-Catalyzed Hydrolysis of α-N-Benzoyl-L-Arginine Ethyl Ester and α-N-Benzoyl-Argininamide, *J. Am. Chem. Soc. 87*, 2728−2737.
28. Frankfater, A., and Kuppy, T. (1981) Mechanism of Association of N-Acetyl-L-Phenylalanylglycinal to Papain, *Biochemistry 20*, 5517−5524.
29. Weiss, P. M., Cook, P. F., Hermes, J. D., and Cleland, W. W. (1987) Evidence from Nitrogen-15 and Solvent Deuterium Isotope Effects on the Chemical Mechanism of Adenosine Deaminase, *Biochemistry 26*, 7378−7384.
30. Brocklehurst, K., Kowlessur, D., Patel, G., Templeton, W., Quigley, K., Thomas, E. W., Wharton, C. W., Willenbrock, F., and Szawelski, R. J. (1988) Consequences of Molecular Recognition in the S1−S2 Region of Papain for Catalytic Chemistry, *Biochem. J. 250*, 761−762.
31. Hanzlik, R. P., Zygmunt, J., and Moon, J. B. (1990) Reversible Covalent Binding of Peptide Nitriles to Papain, *Biochim. Biophys. Acta 1035*, 62−70.
32. Born, T. L., and Blanchard, J. S. (1999) Enzyme-Catalyzed Acylation of Homoserine: Mechanistic Characterization of the *Escherichia coli* metA-Encoded Homoserine Transsuccinylase, *Biochemistry 38*, 14416−14423.
33. Rudolph, J. (2002) Catalytic Mechanism of Cdc25, *Biochemistry 41*, 14613−14623.
34. Case, A., and Stein, R. L. (2003) Kinetic Analysis of the Action of Tissue Transglutaminase on Peptide and Protein Substrates, *Biochemistry 42*, 9466−9481.
35. Quinn, D. M., and Sutton, L. D. (1991) in *Enzyme Mechanism from Isotope Effects* (Cook, P. F., Ed.) pp 73−126, CRC Press, Boston, MA.
36. Lewis, C. A., Jr., and Wolfenden, R. (1977) Antiproteolytic Aldehydes and Ketones: Substituent and Secondary Deuterium Isotope Effects on Equilibrium Addition of Water and Other Nucleophiles, *Biochemistry 16*, 4886−4890.
37. Bone, R., and Wolfenden, R. (1985) Solvent Isotope Effect on Formation of Protease Complexes with Inhibitory Aldehydes, with an Appendix on the Determination of Deuterium Fractionation Factors by NMR, *J. Am. Chem. Soc. 107*, 4772−4777.

BI052135T